Rational Design of Photoelectrodes for the Fully Integrated Polymer Electrode Membrane - Photoelectrochemical Water-Splitting System: A case study of Bismuth Vanadate

Georgios Zafeiropoulos[1,], Purushothaman Varadhan[1,*], Hannah Johnson[2,4], Lars Kamphuis[1], A. Pandiyan[1], Sachin Kinge[2], Mauritius C.M. van de Sanden[1,3], Mihalis N. Tsampas[1,#]*

[1]Dutch Institute for Fundamental Energy Research-DIFFER, 5612AJ Eindhoven, The Netherlands

[2]Toyota Motor Europe NV/SA, Hoge Wei 33, 1930 Zaventem, Belgium

[3]Department of Applied Physics, Eindhoven University of Technology, 5600 MB Eindhoven, The Netherlands

[4]Laboratory for Molecular Engineering of Optoelectronic Nanomaterials, École Polytechnique Fédérale de Lausanne (EPFL), Station 6, 1015 Lausanne, Switzerland

**First and second authors have contributed equally and possess the first authorship of this article.*

 # - Corresponding Author – m.tsampas@differ.nl

Accepted Version

Abstract

Photoelectrochemical (PEC) reactors based on polymer electrolyte membrane (PEM) electrolyzers are an attractive alternative to improve scalability compared to conventional monolithic devices. To introduce narrow band-gap photoabsorbers such as $BiVO_4$ in PEM-PEC system requires cost-effective and scalable deposition techniques beyond those previously demonstrated on monolithic FTO-coated glass substrates, followed by the preparation of membrane electrode assemblies. Herein, we address the significant challenges in coating narrow band-gap metal-oxides on porous substrates as suitable photoelectrodes for the PEM-PEC configuration. In particular, we demonstrate the deposition and integration of W-doped $BiVO_4$ on porous conductive substrates by a simple, cost-effective, and scalable deposition based on the SILAR (successive ionic layer adsorption and reaction) technique. The resultant W-doped $BiVO_4$ photoanode exhibits a photocurrent density of 2.1 $mA \cdot cm^{-2}$, @ 1.23 V vs. RHE; the highest reported so far for the $BiVO_4$ on any porous substrates. Further, we integrated the $BiVO_4$ on the PEM-PEC reactor to demonstrate the solar hydrogen production from ambient air with humidity as the only water source, retaining 1.55 $mA \cdot cm^{-2}$, @ 1.23 V vs. RHE. The concept provides insights into the features necessary for the successful development of materials suitable for the PEM-PEC tandem configuration reactors and the gas-phase operation of the reactor, which is a promising approach for low-cost, large-scale solar hydrogen production.

Keywords: Photoelectrochemical water-splitting, porous substrate, $BiVO_4$ photoanodes, SILAR method, membrane photoelectrode assembly, Aquivion.

Accepted Version

Introduction

The intermittent nature of solar energy creates an inherent mismatch between photovoltaic (PV) energy production and consumption, limiting the degree to which we can depend on it for the electrical grid.[1–3] In this regard, chemical storage of this energy through solar-driven photoelectrochemical (PEC) splitting of water into hydrogen is a viable alternative that has the potential to realize an affordable and stable power source.[4–7] Although PEC solar to hydrogen efficiencies of up 19% have already been achieved,[6] the conventional monolithic device design causes high ionic resistance with a rapid drop in current density upon scale-up with a typical device size of 1 cm^2.[8,9] From the perspective of developing compact and fully-integrated PEC reactor design, the use of a polymer electrolyte membrane (PEM) as inspiration is of great interest due to its operation at high current density and avoids any internal recombination of hydrogen and oxygen, allowing safe operation which is an essential issue in electrolysis and photoelectrolysis systems.[10–12] Moreover, the stability of the photoelectrodes in PEM configuration is expected to be higher since the material are in contact with polymeric membranes and not with corrosive aqueous electrolytes, and in principle, pure water or water-vapor flowing through the reactor could be sufficient to drive the reactions.[11,12]

In the literature, a few research groups have attempted to employ PEM-PEC reactors for water-splitting applications.[11–19] In these reports, commercially available metal meshes such as Ti, W were partially oxidized to form a core-shell structure consisting of an outer photoelectrode (TiO_2, WO_3) and an inner core of electron-conducting (Ti, W) substrate. Our group has previously demonstrated the wide-band gap (TiO_2, WO_3) based PEM-PEC hydrogen production,[11,12] however the incorporation of narrow-bandgap semiconductor for better light harvesting characteristics are lacking till date. Further, we demonstrated the surface functionalization of photoanodes to absorb the humidity from the air to perform the gas-phase water splitting reaction that produces hydrogen from ambient air. However due to the wide band-gap of TiO_2, and WO_3, the overall efficiency of the system is limited and hence it is essential to develop systems based on narrow band-gap semiconductors.

Among various semiconductor materials, bismuth vanadate ($BiVO_4$) has emerged as one of the most promising photoanode candidates.[20–24] because of its outstanding advantages, including a relatively narrow band-gap (~2.4 eV), suitable band alignment to water redox reactions, and reasonable stability in an aqueous environment, etc. However, the charge carrier

Accepted Version

separation/transfer in $BiVO_4$ is believed to be slow due to a small polaron hopping conduction mechanism resulting in a considerable conduction activation energy and relatively sluggish electron mobility. [23,24] Several attempts have been made to overcome this slow electron transport and improve electron collection by introducing n-type dopants (W^{6+} or Mo^{6+}) [20–23,25,26], which substitutes the V^{5+} and increase the n-type carrier density. Further, co-catalysts such as NiOOH, FeOOH, cobalt phosphate,[20,22,27] have been integrated on the $BiVO_4$ to mitigate the sluggish charge-carrier dynamics for the oxygen evolution reaction (OER). $BiVO_4$ based photoanodes have been reported with photocurrent densities up to 6.72 $mA.cm^{-2}$, which is about 90% of the maximum theoretical current density of 7.5 $mA.cm^{-2}$ under AM1.5G illumination (100 mW cm^{-2}).[25]

Historically, transparent conducting oxides, particularly fluorine-doped tin-oxide (FTO), are preferred for the deposition of $BiVO_4$ photoanodes.[20,21,28] However, integrating the photoelectrodes deposited on monolithic FTO-coated glass substrates is not straightforward in large-scale electrolyzers due to the absence of charge carrier transportation path across the substrate and the membrane, causing ionic transfer resistances.[26] Hence, further modifications are vital, and in particular, $BiVO_4$ has to be deposited on the substrates that can be coupled with the PEM electrolyzer. In simple terms, most of the cost-effective photoelectrodes (including $BiVO_4$ developed so far), use substrates which need further modifications to be able to integrated into a compact electrolysis system. They would further require a significant research effort to be integrated into real-world solar fuel systems.

In our previous work, sputter deposited W thin-films on porous Ti-felt was converted into WO_3 by anodization technique followed by the $BiVO_4$ deposition.[29] Such $BiVO_4/WO_3$ porous photoanodes was used for the visible light driven PEC water-splitting. Further, Amano et.al., reported the surface functionalization of various photoanodes with Nafion ionomer for the water-absorption purpose, to drive the water-vapor fed hydrogen generation.[13,30–32] Similar works has also been reported by other research groups,[33] where Nafion ionomer has been used for the water-absorption purpose to drive the water-splitting reactions. In our previous work we demonstrated the significant advantages of novel Aquivion ionomer which has better water-absorption characteristics and stability over Nafion.[11] With this demonstration we realize the importance of combining the narrow-band gap $BiVO_4$ photoanodes with the Aquivion ionomer, to demonstrate the water-vapor fed hydrogen generation under atmospheric humidity level (<100%).

Accepted Version

Here, we developed $BiVO_4$ on porous substrates that can function both in conventional liquid phase and can also be readily integrated into the compact MEA based PEC-water splitting system. In particular, we chose Ti-felt as substrate to be both active in charge carrier transport across the substrate and its natural porosity that allows light transmittance for the complimentary light absorption by the counter photoelectrode.[11] The resultant W doped $BiVO_4$ on Ti-felt porous substrate developed herein demonstrates excellent PEC performance with a current density of 2.1 $mA \cdot cm^{-2}$ @ 1.23 V vs. RHE. Further, we functionalized the $BiVO_4$ photoelectrode by the impregnation of appropriate ionomers to absorb the moisture from air and demonstrated the water-vapor fed PEC water splitting. The functionalized W: $BiVO_4$ integrated on PEM-PEC reactor shows excellent gas-phase performance at the relative humidity (RH) of 60 and 100% with a current density of 1.1 and 1.55 $mA.cm^{-2}$, respectively, corresponding to 51 and 70%, respectively, of the current density obtained from the liquid phase PEC water-splitting.

Rational designing of the photoelectrodes for membrane electrode assembly reactor

The rationale behind the design of photoelectrodes suitable for the membrane electrode assembly is represented as the schematic illustration (Schematic 1a and 1b). In a typical photoelectrode design the light-absorbing material and the co-catalysts are integrated on the top surface of the substrate whereas the other part of the substrate does not contribute for the charge carrier transport across the membrane thus limiting the integration of such photoelectrodes into the PEM-PEC devices as shown in Schematic 1a.

Accepted Version

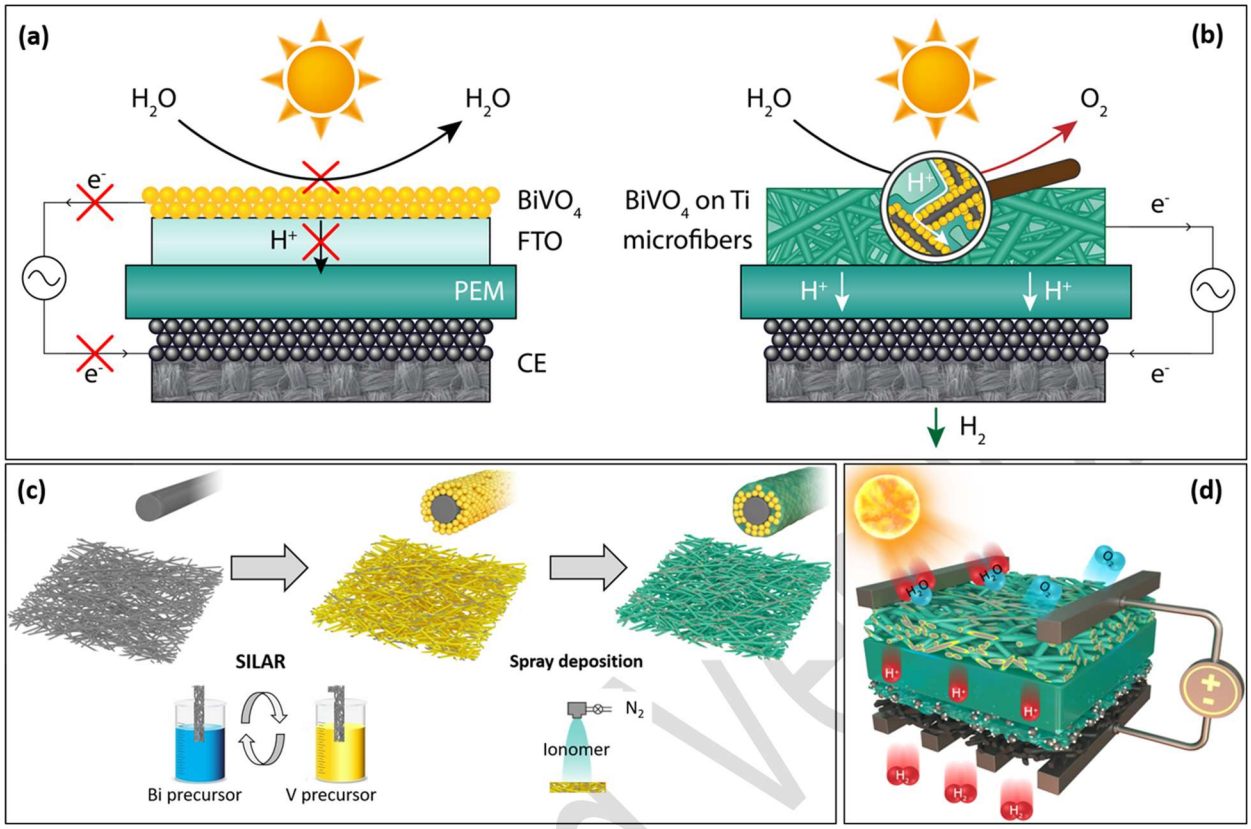

Schematic 1| Rational design of photoelectrodes Schematics 1: **a,** Schematic representation on the conventional approach for photoanode preparation, in which the $BiVO_4$ is deposited on top of monolithic FTO-coated glass substrates, which is not suitable for the integration into a PEM electrolysis system whereas, **b,** represents the $BiVO_4$ photoanodes deposited on the porous light penetrable substrates ideal for the PEM electrolysis. **c,** shows the deposition of $BiVO_4$ on porous substrates by s-SILAR method and functionalization by Aquivion ionomer, **d,** shows the 3D view of fully integrated photoelectrode and the dark-electrode on the PEM-PEC with the charge-transfer dynamics of the overall water-splitting process.

In contrast, Schematic 1b shows the multi-functional photoelectrode device proposed, in which the light-harvesting component and the co-catalysts are integrated on the top surface of the substrate, whereas the porous nature of the substrate allows the charge-transfer (proton) across the membrane enabling integration into PEM-PEC devices.

Accepted Version

Development of $BiVO_4$ on PEM-PEC suitable substrates by s-SILAR:

In literature, $BiVO_4$ thin films have been deposited by various methods including electrochemical deposition,[20,34] spin-coating,[35] reactive sputtering,[36] dip-coating,[37,38] and hydrothermal methods.[39] Out of these, electrochemical deposition of $BiVO_4$ on FTO-coated glass substrate has been the most successful with the highest current density and stability reported so far.[20,34] However, the electrochemical deposition method is sensitive to the electrolyte purity, environment, and applied bias. While studies of such high-performance composite photoanodes are undoubtedly important and demonstrate the potential of $BiVO_4$ for use in practical solar water splitting cells, investigation of simpler and cheaper deposition methods is also warranted.

Herein we employ cost effective, scalable and ease of use technique known as successive ionic layer adsorption and reaction (SILAR) which is the modified form of simple dip-coating for the preparation of $BiVO_4$ thin film.[37,38] In particular, we use a simplified-SILAR (s-SILAR) method in which there are rinse steps (which are typical used in SILAR procedures) in the process of film preparation as shown in Schematic 1c. We replaced the conventional FTO-coated glass substrate with a porous conductive Ti-felt substrate to enable the photoanode for the direct integration on the PEM-PEC reactor. For comparison, we have also deposited $BiVO_4$ on FTO-coated glass and W-mesh to demonstrate the suitability of the s-SILAR deposition techniques over various substrates. The exact preparation method of $BiVO_4$ by the s-SILAR technique is provided in the Experimental section. As noted earlier, for $BiVO_4$ its low electron conductivity is a critical factor limiting the charge transport,[23,24] and so doping has widely been used to improve the performance. W^{6+} and Mo^{6+} dopants have been shown to enhance the electron conductivity and the electron density.[22–24] Here we use W^{6+} as a dopant due to its enhanced performance and stability in liquid electrolytes.[23,24,29,39,40] We have carried out the s-SILAR deposition of $BiVO_4$ with varying W dopant (0-5%) concentration. The optimum doping level of W in $BiVO_4$ (to achieve the highest photocurrent density) is 3%, which matches well with the reported results (~2-3% of W loaded $BiVO_4$).[23] Further the ideal deposition conditions in terms of s-SILAR dipping cycles was found to be 10 cycles. All the optimization process and the results with various doping levels and deposition cycles are provided in the supplementary information (Supplementary Figure S1).

Accepted Version

Results and Discussion

First, the $BiVO_4$ photoanodes were characterized by the photocurrent density-potential (J−V) to find the optimum dopant (W) loading levels. The results reveal that 3% W doped $BiVO_4$ (W:$BiVO_4$) shows the highest current density (discussed in PEC section), which agrees well with the previous reports. [23] In the main text of the manuscript, we provide the characterization and discussion based on the optimum (3%) W:$BiVO_4$ and undoped $BiVO_4$. The morphology of as-prepared photoanodes is characterized by scanning electron microscopy (SEM) and transmission electron microscopy (TEM). Figure 1a-c shows the SEM images of s-SILAR deposited W:$BiVO_4$ on the Ti-felt substrate. All the images reveal a worm-like structure with a diameter in the range of 50-100 nm (inset of Figure 1 c) and are uniformly distributed over the substrate. Varying the dopant concentrations of W from 0 - 5% results in similar morphologies with no visible changes on the structure, size and distribution over the substrate. To confirm the existence of element W in the W:$BiVO_4$ film, EDX mapping on the top of the film was done, as shown in Figure 1d-f, which demonstrates that the Bi, V, and W elements are uniformly distributed throughout the sample. Figure 1g shows the TEM image of W:$BiVO_4$ particles, and figure 1h shows the selected area electron diffraction (SAED) pattern from the cluster of particles. The SAED pattern shows multiple angle diffractions from the various surface of the particles with dominant diffractions from (002), and (200), as expected from the $BiVO_4$.[41] Figure 1h shows the high-resolution TEM image, and figure 1f shows the lattice resolved image of a single particle. The distance measured between two adjacent lattices from the high-resolution image has a lattice spacing of 0.36 nm which corresponds to the (200) plane of $BiVO_4$.[42]

Accepted Version

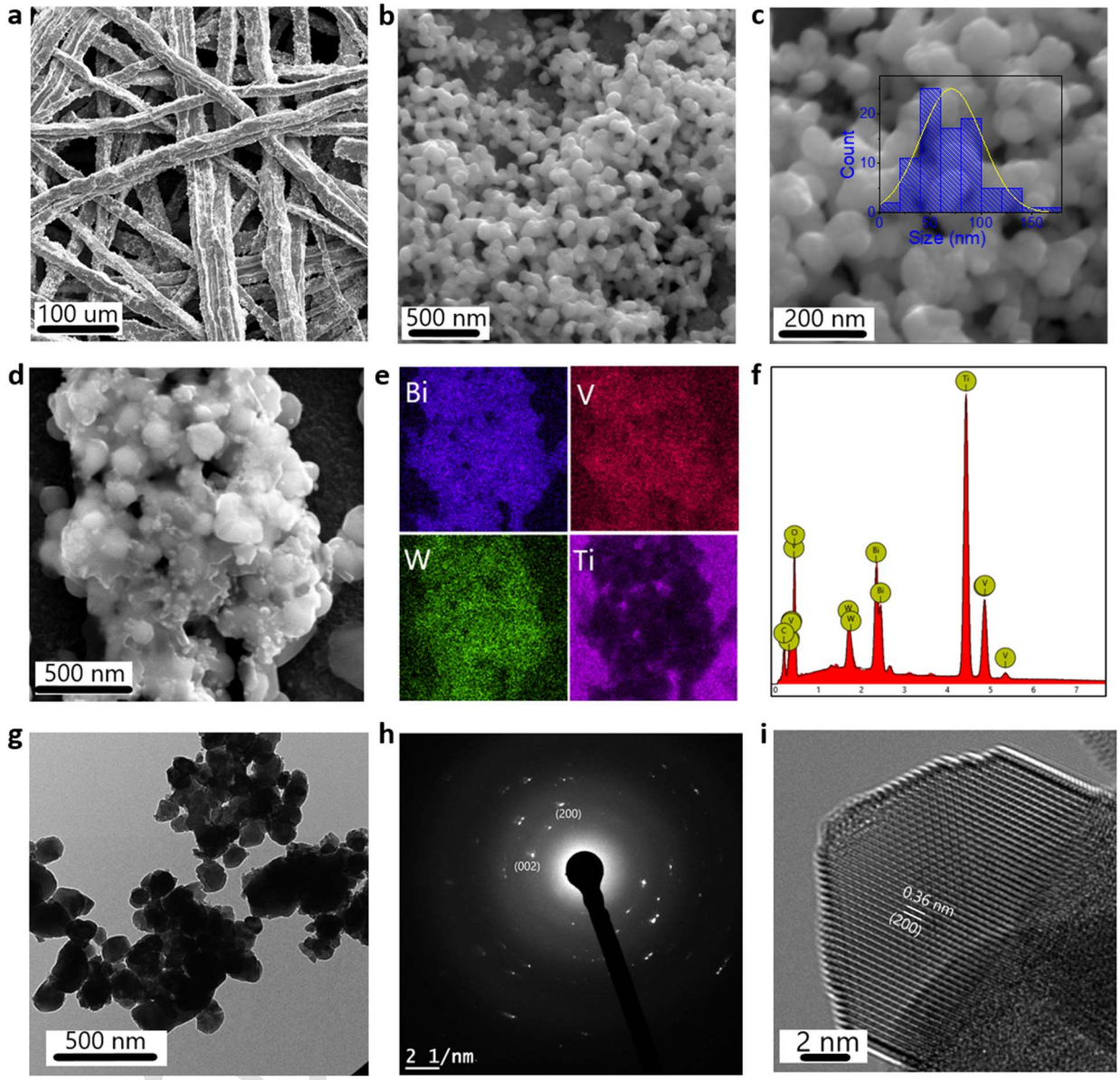

Figure 1|Electron microscopy characterization of $BiVO_4$. a, b, and **c,** show the SEM images of 3% W:$BiVO_4$ deposited on the Ti-felt. **d,** shows the part of the SEM image used for energy-dispersive x-ray spectroscopy (EDX) mapping. **e,** and **f,** shows the EDX mapping, and spectrum of W:$BiVO_4$, respectively. **g,** shows the TEM image. **h,** shows the selected area electron diffraction (SAED) pattern from the cluster of $BiVO_4$ particles, and **i,** shows the lattice resolved image of single $BiVO_4$ particle.

Further, the crystal structure of the films was determined by X-ray diffraction (XRD). XRD reveals (Figure 2a) that all the films are pure monoclinic scheelite phase, which is the most photochemically active phase of $BiVO_4$.[43] The peaks were obtained at 2θ = 19.05, 28.90, 30.85, 34.90 degrees, corresponding to (110), (121), (040), (200), and (020), respectively. The diffraction pattern matches well with JCPDS card no. 14-0688, confirming formation of the monoclinic phase of $BiVO_4$. Further, the dominant peak (200) planes match well with the SAED and lattice resolved HRTEM image. We did not observe any shifts on the diffraction peaks for different loadings of W (Supplementary Figure S2), which is in consistent with prior reports.[23,43] X-ray photoelectron spectroscopy (XPS) was used to investigate the surface electronic properties and chemical states of $BiVO_4$. As shown in Figure 2b, XPS survey spectra (Shirley background corrected) reveals the presence of Bi, V, O, W, and C elements on the surface of the $BiVO_4$ film (Figure 2b).[23,39,44] Further, the high-resolution XPS spectra for the core-level of Bi 4f, V2p, O1s and W4f for undoped and W:$BiVO_4$ was recorded (Figure 2c). Lorentzian deconvolution were used for data fitting and the two peaks at the binding energy levels of 158.7 and 164.0 eV corresponds to the Bi $4f_{7/2}$ and Bi $4f_{5/2}$ of Bi 4f levels.[45] The peak positions are at much higher level than that of metallic Bi, i.e. 156.8 and 162.2eV, which indicates the presence of Bi +3 state at the surface of the film. Meanwhile, the peaks at 516.4 eV and 524.0eV, corresponds to the V $_2p_{3/2}$ and V $_2p_{1/2}$, respectively, with the split energy of 7.6eV, occurring at the natural features of V at +5 oxidation state (Figure 2d).[46,47] The deconvolution applied to the O 1s spectrum (Figure 2e) shows the occurrence of oxygen species in various forms. The peak at ~530 eV is ascribed to the O1s levels due to the oxygen in the lattice structure,[48] whereas the peaks at ~532 eV can be attributed to the non-lattice and chemisorbed oxygen or dissociated oxygen from water molecules, which might enhance the photo-electrocatalysis.[42,48–50] Finally, the presence of W dopant in $BiVO_4$ lattice is established by the presence two peaks at 35.6 and 37.7 eV levels for W:$BiVO_4$ which corresponds to the W $4f_{5/2}$ and W $4f_{7/2}$, whereas the undoped $BiVO_4$ shows no such peaks (Figure 2f).[50]

Accepted Version

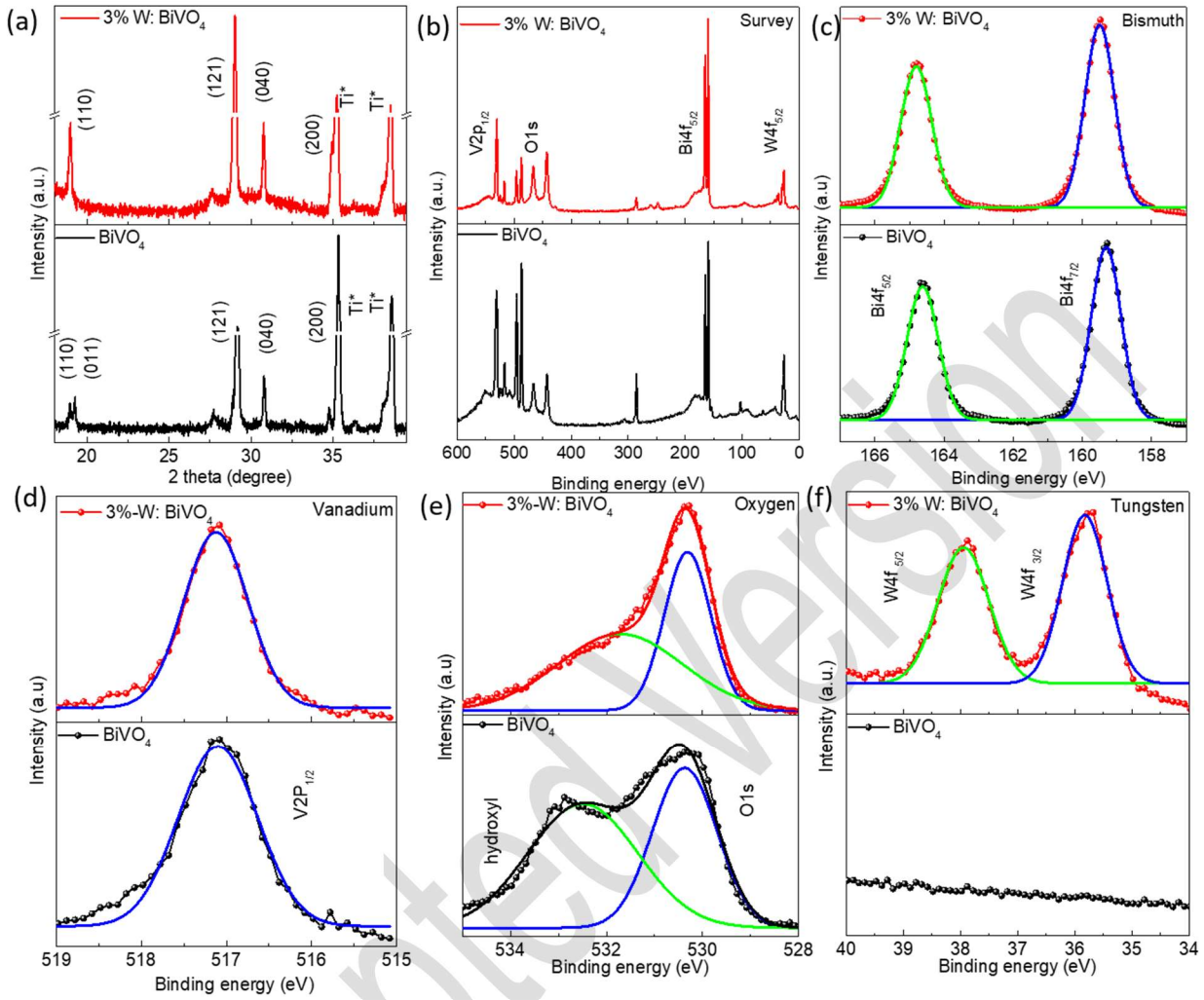

Figure 2| Materials characterization. a, X-ray diffraction of bare Ti-felt, $BiVO_4$ and 3% W-$BiVO_4$ – the dashed lines represent the $BiVO_4$ (121) and (040) planes. X-ray photoelectron spectroscopy (XPS) of undoped and 3% W: $BiVO_4$ on Ti-felt. **b,** survey spectrum, **c,** Bi 4f, **d,** V2p, **e,** O1s, and **f,** W 4f.

Accepted Version

Conventional photoelectrochemical measurements

The photocurrent density-potential (J−V) curves of $BiVO_4$ photoanodes deposited on various substrates were obtained by chopped linear sweep voltammetry (LSVs) measurements. For all the presented results the samples were illuminated with AM1.5G (100 mW cm^{-2}) light, and all the measurements were carried out in 0.1 M sodium sulfate solution with pH~6.0. The photocurrent densities were scanned over an appropriate potential window for undoped and W:$BiVO_4$ photoanodes on Ti-felt substrates and the results are shown in Figure 3a.

Undoped $BiVO_4$ shows a photocurrent density of 0.5 $mA \cdot cm^{-2}$ at 1.23 V versus RHE; for reference, its theoretical photocurrent of 7.5 mA cm^{-2} can be derived from its light absorption curve. With the successful doping of different concentrations, the current density increases first and then decreases as the percentage of W is increased (Supplementary Figure S1).

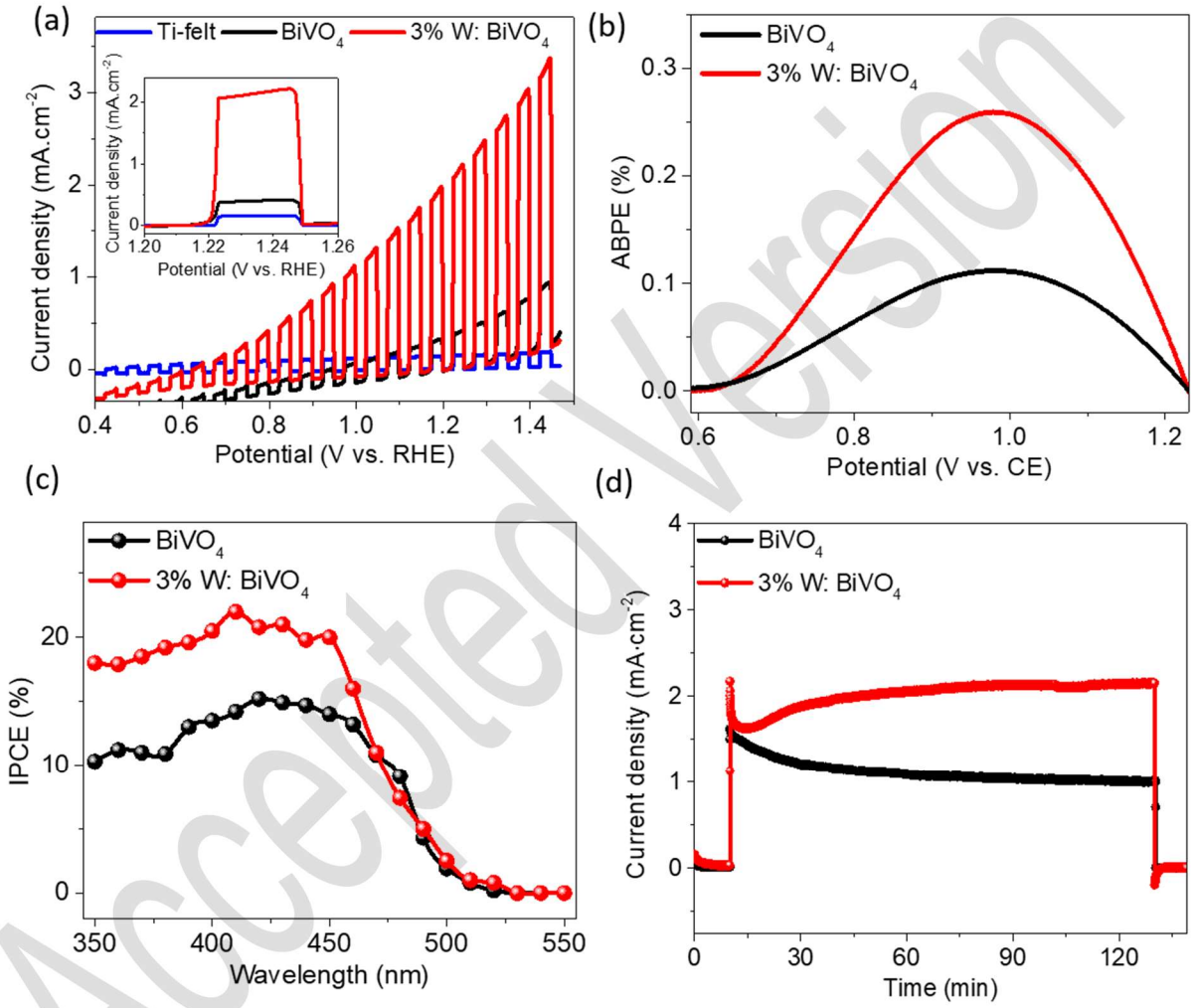

Figure 3| Photoelectrochemical water-splitting characteristics in conventional liquid phase. **a,** LSV curves, **b,** Applied bias to photon conversion efficiency, **c,** Incident photon-to-current conversion efficiency (IPCE measured at a bias of 1.23 V vs RHE, and **d,** Chronoamperometric analysis on the long-term stability of undoped and W: $BiVO_4$. All the results were measured under a three-electrode system in 0.1 M sodium sulfate solution, pH = 6.0 as the electrolyte under one sun illumination.

Accepted Version

As expected, the intermediate W doping (3% of W) leads to the highest photocurrent of 2.1 $mA \cdot cm^{-2}$ at 1.23 V versus RHE, alongside with a ~50 mV cathodic shift in the onset potential.[23] As the dark currents are not increased compared with the dark currents obtained in undoped $BiVO_4$, it is safe to conclude that the enhanced photocurrents in the composite photoanodes mainly originate from the improved photoconversion efficiency. The performance of the photoanode can be further enhanced by integrating the suitable co-catalysts,[20] however we refrain from such addition as most of the known co-catalysts are unstable in acidic conditions that exists in PEM configuration. Further development and integration of acid stable OER electrocatalyst suitable for $BiVO_4$ could be used to enhance the photocurrent density and onset potential of the photoanode. Here we employed 0.1 M sodium sulfate solution as the electrolyte in order to compare the results directly with the reported literature (Table S1). The current densities reported herein are the highest for $BiVO_4$ on any alternative MEA suitable substrates. We also deposited W:$BiVO_4$ on FTO-coated glass substrate, and porous W-mesh substrate for comparison and demonstration purpose. The structural and PEC characterizations of $BiVO_4$ deposited on alternative substrates has been carried out and the results are provided in the supplementary information (Figure S2-S6). $BiVO_4$ deposited on alternative substrates reveal the excellent PEC and structural characteristics, suggesting that the s-SILAR method is simple, cost-effective and extendable to any alternative large area substrates and can be easily adopted to industrial production.

The efficiency of the undoped and W:$BiVO_4$ photoanode were further assessed through the applied bias photon-to-current efficiency (ABPE). The ABPE of the photoanodes are calculated from the LSV curves measured (two-electrode with Pt as a counter electrode (CE), assuming 100% Faradic efficiency, as shown in Figure 3b. At an applied potential of about 0.9 V vs. CE, a maximum ABPE of 0.27% has been achieved for W:$BiVO_4$. Moreover, the high efficiency achieved at a potential as low as 0.95 V vs. CE indicates its promise as a photoanode in a tandem configuration and it should be noted that with the integration of cocatalysts the ABPE value can be enhanced significantly.[51] To further elucidate the spectral response of $BiVO_4$ photoelectrode on the PEC performance, we measured the half-cell solar to hydrogen (IPCE) spectra with a three-electrode measurement (Figure 3c). The IPCE value is defined as following equation 1:[51]

$$\mathrm{IPCE} = \frac{1024 \times \mathrm{J_H(mA/cm^2)}}{\lambda(\mathrm{nm}) \times \mathrm{P_{ph}(mW/cm^2)}} \times 100\% \quad (1)$$

in which λ is the wavelength of the illuminating monochromatic photons, and P_{ph} is the power

Accepted Version

of the incident photons. The IPCE value of W:$BiVO_4$ reaches about ~20.8% at 420 nm - that is ~1.3 times higher than that of undoped $BiVO_4$ photoanode (~15.2%).

The PEC stability of undoped and W:$BiVO_4$ photoanode was measured by chronoamperometry (CA) J_p– t curve at 1.23 V vs. RHE for two hours, and the results are shown in Figure 3d. It can be seen that the photocurrent density of W:$BiVO_4$ photoanodes initially reduces and increases to stabilize around ~ 2.1 $mA.cm^{-2}$, matching well with the LSV curve. The behavior of the W-doped samples in the initial period of time can be attributed to the photocharging of $BiVO_4$ as reported earlier.[52] However further experimental evidences are necessary to conclude the role of dopants and how it affects such photo charging. The degradation of undoped BiVO4 has been well-studied in the literature,[20-24] along with co-catalyst integration and surface protection strategies to enhance the stability. Additionally however, doping itself, has not only been shown to enhance the performance but also the stability and indeed, the enhanced stability of doped $BiVO_4$ photoanodes compared to the undoped $BiVO_4$ has been previously reported.[53] Overall, the W:$BiVO_4$ on Ti-felt demonstrates excellent performance, including the onset potential, current density, and stability.

Photoelectrode integration into the membrane-electrode-assembly setup

Most of the published laboratory scale PEC studies for metal-oxide photoanodes including $BiVO_4$ have been measured with the conventional liquid electrolyte based 3-electrode measurements in a beaker or in an H-cell configuration.[54] Though such analyses are simple, effective and attractive in laboratory scale, development of a large-scale and commercially viable PEC system requires an alternative approach. Feasible gas separation approaches such as membrane integration must be developed, as demonstrated in commercial alkaline or PEM electrolyzers.[55–57]

In particular PEM-based PEC is more attractive as the system can operate with relatively high current density, near-neutral electrolytic conditions, and also operate with water-vapor from the humidity in the ambient air. With all such considerations, here we interfaced the $BiVO_4$ photoelectrode deposited on a porous substrate in a membrane-electrode assembly setup, with Aquivion® membrane (150 μm thick, E98-15S, Sigma-Aldrich) and commercial Pt/C as the counter electrode. It should be noted that the Pt-group counter electrodes can well be replaced with cost-effective electrocatalysts,[56,58] which are commercially available and here we use Pt-group materials for the purpose of representation and simplicity. Only limited studies were reported in

Accepted Version

employing the solar-driven water splitting with a PEM reactor design and, in particular, for gas-phase water splitting. As a result, there is no standard for evaluating the PEC properties under gas-phase operation. Hence, in our previous report, we established an experimental protocol for benchmarking the activity of the photoelectrodes.[11]

PEC characteristics of fully integrated reactor and hydrogen from humid air

To achieve water-vapor fed operation of PEM-PEC is attractive (Figure 4a), functionalization of the photoanode is required to capture the water vapor from the humidified air. Our group has already demonstrated the surface functionalization of photoanodes and in-depth analysis on the photoanode characteristics by the deposition of different ionomers (Nafion and Aquivion) to absorb the moisture.[11] Based on our previous studies, we employed an Aquivion based ionomer here as it possesses i. better light-transparency in the visible region, ii. higher absorbance of water-vapor, and iii. better PEC stability of the photoanode. Schematic and SEM images of the cross-sectional view of all the layers involved in the PEM-PEC arrangements are shown in Figure S8. More details of the impregnation of Aquivion ionomer on the photoanode and the gas phase operation are given in the Experimental section.

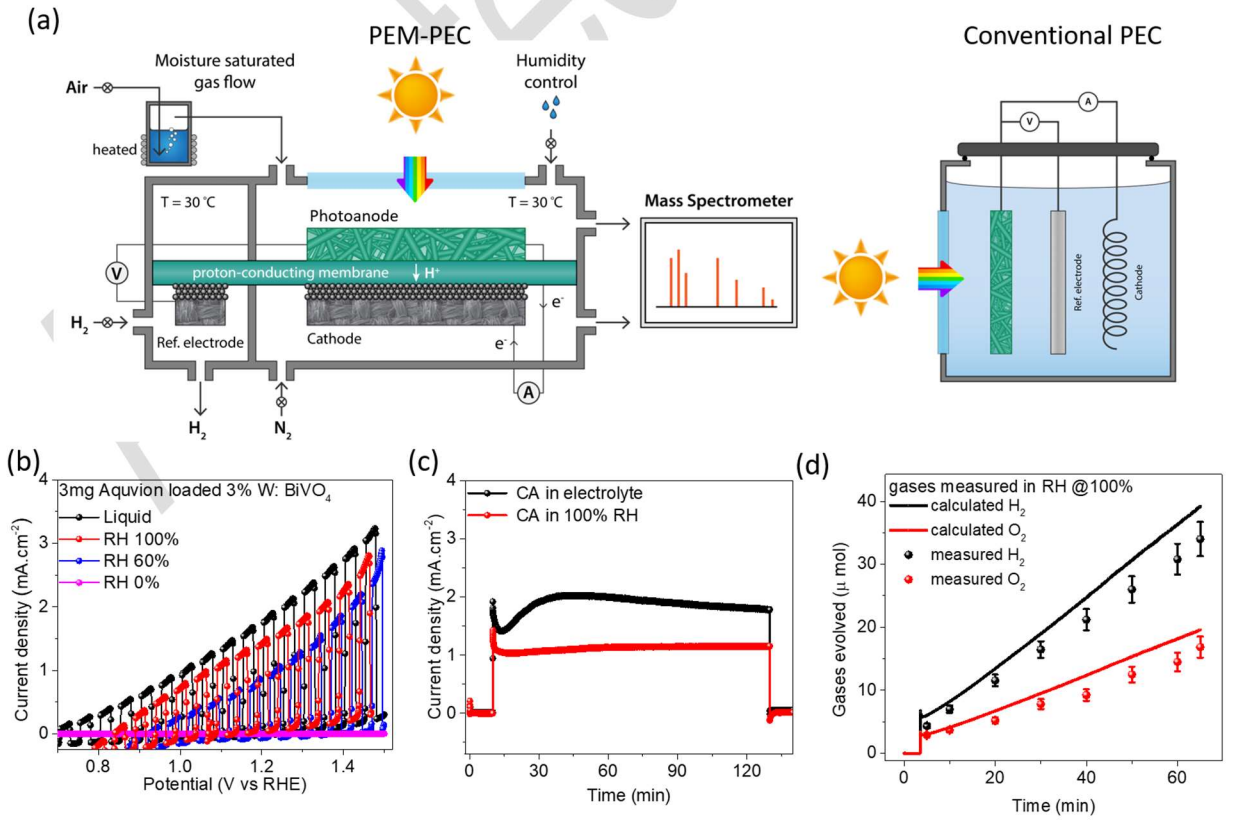

Accepted Version

Figure 4| Fully-integrated zero-gap photoelectrode for the air to hydrogen. **a**, PEM-PEC experimental configuration used for evaluating the photoanodes with a standard hydrogen reference electrode with the capability to operate under a humidified air with varying humidity levels (left). Conventional PEC reactor on the right**. b,** LSV curves of functionalized (3 mg·cm^{-2} Aquivion loaded) W:$BiVO_4$ under chopped light illumination at various RH and **c,** Chronoamperometric analysis on the long-term stability of functionalized W:$BiVO_4$ measured at 1.23 V vs. RHE. **d,** H_2 and O_2 evolution detected from functionalized W:$BiVO_4$ by MS and the calculated amounts of H_2 (black dash line) and O_2 (red dash line) under RH 100%.

Figure 4b shows LSVs obtained under various relative humidity levels of functionalized W:$BiVO_4$ deposited on Ti-felt. As shown in Figure 4b, with 0% RH (dry air), no photocurrent density is visible due to the absence of any water (proton) and so there is a failure of contacts within the MEAs. However, with the humidified air, the photoanodes exhibit photocurrent which is enhanced at higher RH. The maximum photocurrent is obtained with 100% RH at which the current density reaches 1.55 mA.cm^{-2} at 1.23 V vs. RHE, which is ~70% of the current density obtained for the same electrode under conventional liquid-based PEC reactor (also shown in the same figure for comparison purpose). The non-zero dark current particularly in the water-vapor fed PEM-PEC reaction can be attributed to the ineffective diode characteristic of the Aquivion ionomer/$BiVO_4$ anode/PEM interface or reductive characteristics of Aquivion ionomer that leads to significant current leakage.[59,60] However, the dark current of the PEC reaction measured in the electrolyte solution is minimal (~25 μA.cm^{-2}) at 1.23 V. The results herein demonstrate that the Aquivion functionalized W:$BiVO_4$ photoanode developed herein has the potential to produce hydrogen from the water-vapor available in the open air by PEC water-splitting. Comparison of the $BiVO_4$-based photoanodes for PEM-PEC water-vapor fed electrolysis reaction is shown in Table S2.

Further, the stability of the photoanodes in the PEM-PEC configuration under the electrolyte and with RH of 100% were carried out and the results are shown in Figure 4c. The results demonstrate that the photoanodes are stable over the period of 2 hours acidic conditions (Ionomers are acidic in nature). Recently Amano et.al., reported that $BiVO_4$ photoanodes are more stable in acidic conditions than the neutral conditions (pH7).[61] In order to confirm that the obtained photocurrent is produced due to the water splitting process, it is important to determine the amount

Accepted Version

of evolved H_2 and O_2 gases. The home-made PEM-PEC reactor built in our laboratory is airtight and acts as a perfect reactor for gas evolution analysis. The PEM-PEC cell was directly connected to the quadrupole mass spectrometer for continuous measurements of gases. As a result, we could simultaneously measure both the photocurrent and the concentration of the evolved H_2 /O_2 gases with minimal error. Figures 4d shows the evolution of the hydrogen and oxygen gases and the simultaneously recorded photocurrent over time under the RH 100%. The experiment was conducted at 1.23 Vs. RHE under AM1.5 simulated solar light. The J_p-t curve was recorded during the gas evolution time to calculate the theoretical gas production rates. The produced H_2 and O_2 measured under electrolyte are 30.8 μmol cm^{-2} and 14.2 μmol cm^{-2} after 60 min, respectively, corresponding to the stoichiometric ratio of ~2:1 for water splitting. Calculated gas evolution curves from the recorded photocurrent match well with the experimentally detected gas evolution. The photoanode reached ≈80% of the faradaic efficiency within the first 15 min and later saturated at 85%, which is a typical value for the $BiVO_4$ based photoanodes.[39] The results show that photocurrent densities measured under the highest relative humidity (RH – 100%) achieve <70% of the current density measured in liquid electrolyte. In addition to H_2 and O_2 no other gases including CO_2 has been detected during the stability of the $BiVO_4$ photoanodes, which shows that the $BiVO_4$ functionalized with Aquivion is stable in the given range of potentials and time. In literature, co-catalysts such as NiOOH, FeOOH, cobalt phosphate were integrated to $BiVO_4$ to achieve the best photooxidation performance, however such co-catalysts are generally unstable in acidic conditions.[20,22,27] It should be noted that the PEM-PEC configuration is acidic in nature due to the direct proton pumping and hence the co-catalyst may not be stable under these conditions. Developing and integrating the acid-stable co-catalysts and improving the water absorption characteristics of ionomers and additives will be a critical future work to bring the performance matching the liquid phase PEC reaction.

Conclusions

Herein we demonstrate the continuous production of green hydrogen by PEC splitting of water vapor in the gas phase. To achieve this, we prepared a $BiVO_4$ photoanode on various porous substrates in the form of a gas-diffusion electrode which allows the integration of a highly efficient photoanode in the PEM electrolysis reactor. The resultant optimum W:$BiVO_4$ on Ti-felt substrate exhibited the highest photocurrent density (2.1 $mA \cdot cm^{-2}$) and stability for $BiVO_4$ on any alternative

Accepted Version

substrates and further improvements are expected with the integration of appropriate co-catalysts. Further, we functionalized the $BiVO_4$ with Aquivion ionomer to adsorb the water molecules from humid air that achieved 70% (1.55 $mA.cm^{-2}$) of the PEC performance in liquid operation at 1.23 V. The design demonstrated herein can be further integrated into the dual photoelectrodes tandem PEC-system in to utilize a larger percentage of the solar spectrum to drive unassisted water-splitting. Such a tandem cell can demonstrate the full potential of PEM-PEC as a low-cost, large-scale and renewable alternative to steam reformed hydrogen, with a large geographical applicability – no need for liquid water supply.

Accepted Version

Experimental Methods

Photoelectrode Preparation: Ti-felt purchased from Bekaert (0.4 mm felt thickness, 20 μm wire thickness, 80% porosity), was cut into 1.5×5 cm^2 and cleaned before the s-SILAR deposition. The cleaning procedure included the ultrasonic cleaning of acetone, ethanol and Millipore water. The s-SILAR deposition process is given below: Bi-precursor containing 200 mL of 0.025 M $Bi(NO_3)_3$, and V-precursor with 200 mL of 0.025 M NH_4VO_3 were used as immersion bath for the s-SILAR deposition as shown in Schematic 1 and Supplementary Figure S7. The Millipore water (>17Ω) was used as the solvent for V-precursor, whereas the mixture of acetic acid and water (1: 19) was employed as the solvent for Bi-precursor. The W doped $BiVO_4$ films were fabricated by adding ammonium metatungstate ($(NH_4)_6H_2W_{12}O_{40}\cdot xH_2O$) to replace the equivalent weight of VO $(acac)_2$. For the fabrication of W doped $BiVO_4$ photoanode (1 % W-$BiVO_4$), molar ratio of W/V was 1%. After ammonium metatungstate was dissolved thoroughly in VO $(acac)_2$ solution, the same s-SILAR deposition process as $BiVO_4$ was conducted. As for the W:$BiVO_4$ photoanodes with different W content (c/c of 3% and 5%), corresponding amount of ammonium metatungstate was added. One cycle of s-SILAR deposition includes immersion of desired substrates into the Bi precursor bath for 30 seconds, followed by the drying of 30 seconds. Subsequently the substrates are immersed into the V bath for another 30 seconds, and the drying of 30 seconds. This process is defined as one s-SILAR cycle. The whole s-SILAR setup is maintained under flowing N_2 during the deposition process. The optimization process has been carried out by varying the SILAR cycles from 5-20 cycles and the best performing photoelectrode was obtained at 10 cycles. All the results discussed herein use 10 SILAR cycles. After all cycles were completed, the film was rinsed with Millipore water and dried gently with flowing N_2. Then, the samples were annealed in air at 550°C for two hours with a heating rate of 2.5 C min^{-1} to form uniform $BiVO_4$ thin films. Finally, the samples were immersed in 1M KOH for 20 minutes to remove the unreacted and excess vanadium. The deposition area is uniformly maintained ~2 cm^2 for all the samples. Indeed, during the annealing process at 550°C in ambient condition we noted,[11,29] that Ti and W forms their corresponding oxide structures. Due to the surface oxidation process, there are possibilities of type II heterojunction formation between the substrate and $BiVO_4$.

Materials Characterization: The microscopic investigations were carried out with the field emission – SEM (Nova Nano SEM NPE218) and high-resolution TEM (Tecnai G2) to understand the surface morphology of the samples. The XRD analysis (Bruker D8) were carried out to analyze

Accepted Version

the structure and crystallinity of samples. The surface chemical compositions and states of the samples were analyzed with the XPS (Physical Electrons Quantum 2000 Scanning Esca Microprob, Al Ka radiation).

Photoelectrode Functionalization: The photoanodes were functionalized by spray deposition of Aquivion ionomers as reported in our previous studies.[11] In simple terms, 1 mL of Aquivion dissolved in 20 mL of ethanol was used as the precursor for the spray deposition and the samples were maintained at 60°C. The Aquivion ionomers were uniformly depoisted over the photoanode surface with the gravity feed spray coater with 5 horizontal and 5 vertical lines of spray per cycle with the total of 10 cycles.

Conventional liquid-phase PEC measurements: A simple beaker-based three-electrode configuration with a Pt wire counter electrode and Ag/AgCl (3M KCl saturated) reference electrode was used for the PEC evaluation in an aqueous electrolyte of 0.1 M sodium sulfate (pH 6.0). The potentiostatic operation was carried out with an electrochemical work station from Ivium (Vertex).The electrode potential versus Ag/AgCl ($E_{\mathrm{Ag/AgCl}}$) was converted to the potential versus RHE (E_{RHE}) by using the following (Nernst) Equation 2.

$$E_{RHE} = E_{Ag/AgCl} + (0.059\,\mathrm{pH} + 0.195)\ \mathrm{V} \quad (2)$$

The PEC performance was measured under an AM 1.5 class A solar simulator (ABET instruments) using a 100 W Xe-arc lamp and calibrated to the illumination intensity of 100 $\mathrm{mW \cdot cm^{-2}}$.

PEM-PEC reactor measurements: The gas-phase PEM-PEC measurement were carried out with the similar method as reported in our previous studies.[11] The Pt (0.5 $\mathrm{mg \cdot cm^{-2}}$) on carbon cloth purchased from FuelCells store were used as the cathode and as the reference electrode for gas-phase operation experiments. A thermostat controlled water-saturator was employed to flow (50 $\mathrm{mL \cdot min^{-1}}$) the water vapor into the reactor. In order to prevent any water condensation, all the external gas connection lines were heated to 90 °C . The system was held for 30 minutes under water-vapor stream before every measurement to maintain the equilibration of the ionomer in the given RH conditions.

Accepted Version

Supporting Information:

ABPE & IPCE calculations, photocurrent densities of $BiVO_4$ for various SILAR deposition cycles, XRD patterns of $BiVO_4$ for various W-doping levels, SEM images of $BiVO_4$ with various SILAR cycles, TEM and EDX of $BiVO_4$, schematic and cross-section SEM image of membrane electrode assembly of photoelectrodes, and table comparing various $BiVO_4$ literature.

Acknowledgments

This research received funding from the Dutch Research Council (N.W.O.) in the framework of the ENW PPP Fund for the top sectors. This research program is co-financed by Toyota Motor Europe. Authors thank E. Langereis (DIFFER) for the illustrations and Laura Gomez Daza, Adrian Labrada Isidro (UCLM), for assisting in the early stages of photoelectrode fabrication by SILAR technique.

Data availability

The data that was used for the plots within this paper and other findings of this study are available from the corresponding author upon reasonable request.

Author Contributions

MNT and H.J. conceived the idea of this study and supervised the research. G.Z. and P.V. synthesized the samples, conducted experiments, analyzed the data, and wrote the manuscript. L.K. performed preliminary experiments of photoanode optimization. A.P. helped with the characterization of the photoanodes. MNT, HJ, RvdS and S.K. secured the funding for the project. All authors discussed the results and commented on the manuscript.

Correspondence and requests for materials should be addressed to MNT.

Competing interests

The authors declare no competing financial interests.

Accepted Version

TOC:

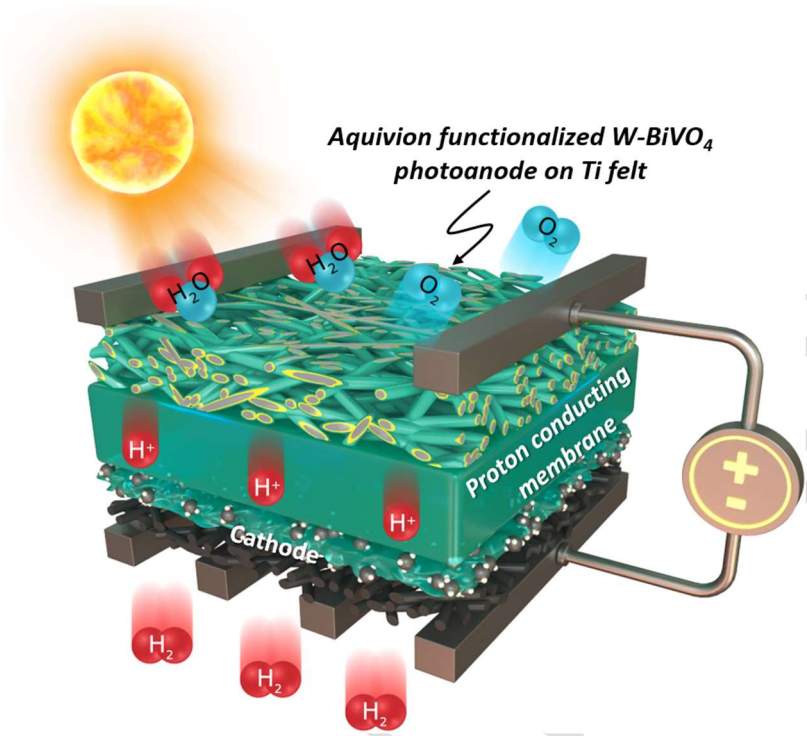

Accepted Manuscript

References:

(1) Orioli, A.; Di Gangi, A. Load Mismatch of Grid-Connected Photovoltaic Systems: Review of the Effects and Analysis in an Urban Context. *Renew. Sustain. Energy Rev.* **2013**, 13–28. https://doi.org/10.1016/j.rser.2012.12.035.

(2) Chu, S.; Majumdar, A. Opportunities and Challenges for a Sustainable Energy Future. *Nature* **2012,** 294–303. https://doi.org/10.1038/nature11475.

(3) Lewis, N. S. Research Opportunities to Advance Solar Energy Utilization. *Science* **2016.** 351(6271). https://doi.org/10.1126/science.aad1920.

(4) Fujishima, A.; Honda, K. Electrochemical Photolysis of Water at a Semiconductor Electrode. *Nature* **1972**, *238* (5358), 37–38. https://doi.org/10.1038/238037a0.

(5) Nocera, D. G. The Artificial Leaf. *Acc. Chem. Res.* **2012**, *45* (5), 767–776. https://doi.org/10.1021/ar2003013.

(6) Cheng, W. H.; Richter, M. H.; May, M. M.; Ohlmann, J.; Lackner, D.; Dimroth, F.; Hannappel, T.; Atwater, H. A.; Lewerenz, H. J. Monolithic Photoelectrochemical Device for Direct Water Splitting with 19% Efficiency. *ACS Energy Lett.* **2018**, *3* (8), 1795–1800. https://doi.org/10.1021/acsenergylett.8b00920.

(7) Hisatomi, T.; Kubota, J.; Domen, K. Recent Advances in Semiconductors for Photocatalytic and Photoelectrochemical Water Splitting. *Chem. Soc. Rev.* **2014,** 7520–7535. https://doi.org/10.1039/c3cs60378d.

(8) Hankin, A.; Bedoya-Lora, F. E.; Ong, C. K.; Alexander, J. C.; Petter, F.; Kelsall, G. H. From Millimetres to Metres: The Critical Role of Current Density Distributions in Photo-Electrochemical Reactor Design. *Energy Environ. Sci.* **2017**, *10,* 346-360. https://doi.org/10.1039/c6ee03036j.

(9) Dilger, S.; Trottmann, M.; Pokrant, S. Scaling Up Electrodes for Photoelectrochemical Water Splitting: Fabrication Process and Performance of 40 cm^2 $LaTiO_2N$ Photoanodes. *ChemSusChem* **2019**, *12*, 1931-1938. https://doi.org/10.1002/cssc.201802645.

(10) Carmo, M.; Fritz, D. L.; Mergel, J.; Stolten, D. A Comprehensive Review on PEM Water Electrolysis. *Int. J. Hydrogen Energy* **2013.** *38 (12),* 4901-4934 https://doi.org/10.1016/j.ijhydene.2013.01.151.

(11) Zafeiropoulos, G.; Johnson, H.; Kinge, S.; Van De Sanden, M. C. M.; Tsampas, M. N. Solar Hydrogen Generation from Ambient Humidity Using Functionalized Porous Photoanodes. *ACS Appl. Mater. Interfaces* **2019**, *11* (44), 41267–41280. https://doi.org/10.1021/acsami.9b12236.

(12) Stoll, T.; Zafeiropoulos, G.; Tsampas, M. N. Solar Fuel Production in a Novel Polymeric Electrolyte Membrane Photoelectrochemical (PEM-PEC) Cell with a Web of Titania Nanotube Arrays as Photoanode and Gaseous Reactants. *Int. J. Hydrogen Energy* **2016**. *41 (40)*, 17807-17817. https://doi.org/10.1016/j.ijhydene.2016.07.230.

(13) Ta, C. X. M.; Akamoto, C.; Furusho, Y.; Amano, F. A Macroporous-Structured WO_3/Mo-Doped $BiVO_4$Photoanode for Vapor-Fed Water Splitting under Visible Light Irradiation.

Accepted Version

ACS Sustain. Chem. Eng. **2020**, *8* (25). https://doi.org/10.1021/acssuschemeng.0c02331.

(14) Zafeiropoulos, G.; Stoll, T.; Dogan, I.; Mamlouk, M.; van de Sanden, M. C. M.; Tsampas, M. N. Porous Titania Photoelectrodes Built on a Ti-Web of Microfibers for Polymeric Electrolyte Membrane Photoelectrochemical (PEM-PEC) Cell Applications. *Sol. Energy Mater. Sol. Cells* **2018**. 180, 184-195. https://doi.org/10.1016/j.solmat.2018.03.012.

(15) Xu, K.; Chatzitakis, A.; Vøllestad, E.; Ruan, Q.; Tang, J.; Norby, T. Hydrogen from Wet Air and Sunlight in a Tandem Photoelectrochemical Cell. *Int. J. Hydrogen Energy* **2019**, *44* (2), 587-593. https://doi.org/10.1016/j.ijhydene.2018.11.030.

(16) Aricò, A. S.; Girolamo, M.; Siracusano, S.; Sebastian, D.; Baglio, V.; Schuster, M. Polymer Electrolyte Membranes for Water Photo-Electrolysis. *Membranes* **2017**, *7* (2), 25. https://doi.org/10.3390/membranes7020025.

(17) Rongé, J.; Deng, S.; Pulinthanathu Sree, S.; Bosserez, T.; Verbruggen, S. W.; Kumar Singh, N.; Dendooven, J.; Roeffaers, M. B. J.; Taulelle, F.; De Volder, M.; Detavernier, C.; Martens, J. A. Air-Based Photoelectrochemical Cell Capturing Water Molecules from Ambient Air for Hydrogen Production. *RSC Adv.* **2014**, *4* (55), 29286-29290. https://doi.org/10.1039/c4ra05371k.

(18) Georgieva, J.; Armyanov, S.; Poulios, I.; Jannakoudakis, A. D.; Sotiropoulos, S. Gas Phase Photoelectrochemistry in a Polymer Electrolyte Cell with a Titanium Dioxide/Carbon/Nafion Photoanode. *Electrochem. Solid-State Lett.* **2010**, *13* (11). https://doi.org/10.1149/1.3465306.

(19) Amano, F.; Mukohara, H.; Shintani, A.; Tsurui, K. Solid Polymer Electrolyte-Coated Macroporous Titania Nanotube Photoelectrode for Gas-Phase Water Splitting. *ChemSusChem* **2019** *12(9)*, 1925-1930. https://doi.org/10.1002/cssc.201802178.

(20) Kim, T. W.; Choi, K. S. Nanoporous BiVO4 Photoanodes with Dual-Layer Oxygen Evolution Catalysts for Solar Water Splitting. *Science.* **2014**, *343* (6174), 990–994. https://doi.org/10.1126/science.1246913.

(21) Kim, J. H.; Jang, J. W.; Jo, Y. H.; Abdi, F. F.; Lee, Y. H.; Van De Krol, R.; Lee, J. S. Hetero-Type Dual Photoanodes for Unbiased Solar Water Splitting with Extended Light Harvesting. *Nat. Commun.* **2016**, 13380. https://doi.org/10.1038/ncomms13380.

(22) Kim, J. H.; Lee, J. S. Elaborately Modified BiVO4 Photoanodes for Solar Water Splitting. *Advanced Materials*. **2019.** *31* (20), 1806938. https://doi.org/10.1002/adma.201806938.

(23) Shi, Q.; Murcia-López, S.; Tang, P.; Flox, C.; Morante, J. R.; Bian, Z.; Wang, H.; Andreu, T. Role of Tungsten Doping on the Surface States in $BiVO_4$ Photoanodes for Water Oxidation: Tuning the Electron Trapping Process. *ACS Catal.* **2018**, *8* (4), 3331–3342. https://doi.org/10.1021/acscatal.7b04277.

(24) Abdi, F. F.; Savenije, T. J.; May, M. M.; Dam, B.; Krol, R. Van De. The Origin of Slow Carrier Transport in $BiVO_4$ Thin Film Photoanodes : *J. Phys. Chem. Lett.* **2013**. *4*, 16, 2752–2757. https://doi.org/10.1021/jz4013257.

(25) Shi, X.; Choi, I. Y.; Zhang, K.; Kwon, J.; Kim, D. Y.; Lee, J. K.; Oh, S. H.; Kim, J. K.; Park, J. H. Efficient Photoelectrochemical Hydrogen Production from Bismuth Vanadate-

Accepted Version

Decorated Tungsten Trioxide Helix Nanostructures. *Nat. Commun.* **2014**, 4775. https://doi.org/10.1038/ncomms5775.

(26) Ahmet, I. Y.; Ma, Y.; Jang, J. W.; Henschel, T.; Stannowski, B.; Lopes, T.; Vilanova, A.; Mendes, A.; Abdi, F. F.; Van De Krol, R. Demonstration of a 50 cm^2 $BiVO_4$ Tandem Photoelectrochemical-Photovoltaic Water Splitting Device. *Sustain. Energy Fuels* **2019**. *3*, 2366-2379. https://doi.org/10.1039/c9se00246d.

(27) Chen, B.; Zhang, Z.; Baek, M.; Kim, S.; Kim, W.; Yong, K. An Antenna/Spacer/Reflector Based Au/$BiVO_4$/WO_3/Au Nanopatterned Photoanode for Plasmon-Enhanced Photoelectrochemical Water Splitting. *Appl. Catal. B Environ.* **2018**. *237*, 763-771. https://doi.org/10.1016/j.apcatb.2018.06.048.

(28) Zahran, Z. N.; Mohamed, E. A.; Haleem, A. A.; Naruta, Y. Efficient Photoelectrochemical O 2 and CO Production Using $BiVO_4$ Water Oxidation Photoanode and CO_2 Reduction Au Nanoparticle Cathode Prepared by In Situ Deposition from Au^{3+} Containing Solution . *Adv. Sustain. Syst.* **2017**. *1* (11), 1700111. https://doi.org/10.1002/adsu.201700111.

(29) Stoll, T.; Zafeiropoulos, G.; Dogan, I.; Genuit, H.; Lavrijsen, R.; Koopmans, B.; Tsampas, M. N. Visible-Light-Promoted Gas-Phase Water Splitting Using Porous WO_3/$BiVO_4$ Photoanodes. *Electrochem. commun.* **2017**. *82*, 47-51. https://doi.org/10.1016/j.elecom.2017.07.019.

(30) Amano, F.; Mukohara, H.; Sato, H.; Ohno, T. Photoelectrochemical Water Vapor Splitting Using an Ionomer-Coated Rutile TiO2 Thin Layer on Titanium Microfiber Felt as an Oxygen-Evolving Photoanode. *Sustain. Energy Fuels* **2019**. 3, 2048-2055. https://doi.org/10.1039/c9se00292h.

(31) Amano, F.; Shintani, A.; Mukohara, H.; Hwang, Y. M.; Tsurui, K. Photoelectrochemical Gas-Electrolyte-Solid Phase Boundary for Hydrogen Production from Water Vapor. *Front. Chem.* **2018**. 6, 598. https://doi.org/10.3389/fchem.2018.00598.

(32) Ta, C. X. M.; Akamoto, C.; Furusho, Y.; Amano, F. A Macroporous-Structured WO3/Mo-Doped BiVO4Photoanode for Vapor-Fed Water Splitting under Visible Light Irradiation. *ACS Sustain. Chem. Eng.* **2020**, *8* (25). https://doi.org/10.1021/acssuschemeng.0c02331.

(33) Modestino, M. A.; Dumortier, M.; Hosseini Hashemi, S. M.; Haussener, S.; Moser, C.; Psaltis, D. Vapor-Fed Microfluidic Hydrogen Generator. *Lab Chip* **2015**, *15* (10). https://doi.org/10.1039/c5lc00259a.

(34) Lee, D. K.; Choi, K. S. Enhancing Long-Term Photostability of BiVO4 Photoanodes for Solar Water Splitting by Tuning Electrolyte Composition. *Nat. Energy* **2018**, *3* (1), 53–60. https://doi.org/10.1038/s41560-017-0057-0.

(35) Xia, L.; Bai, J.; Li, J.; Zeng, Q.; Li, L.; Zhou, B. High-Performance $BiVO_4$ Photoanodes Cocatalyzed with an Ultrathin a-Fe_2O_3 Layer for Photoelectrochemical Application. *Appl. Catal. B Environ.* **2017**. 204, 127-133 https://doi.org/10.1016/j.apcatb.2016.11.015.

(36) Chen, L.; Alarcón-Lladó, E.; Hettick, M.; Sharp, I. D.; Lin, Y.; Javey, A.; Ager, J. W. Reactive Sputtering of Bismuth Vanadate Photoanodes for Solar Water Splitting. *J. Phys. Chem. C* **2013**, *117* (42), 21635–21642. https://doi.org/10.1021/jp406019r.

(37) Haji Yassin, S. N.; Sim, A. S. L.; Jennings, J. R. Photoelectrochemical Evaluation of SILAR-Deposited Nanoporous BiVO4 Photoanodes for Solar-Driven Water Splitting.

Accepted Version

Nano Mater. Sci. **2019**. 2(3), 227-234. https://doi.org/10.1016/j.nanoms.2019.10.003.

(38) Guo, W.; Tang, D.; Mabayoje, O.; Wygant, B. R.; Xiao, P.; Zhang, Y.; Mullins, C. B. A Simplified Successive Ionic Layer Adsorption and Reaction (s-SILAR) Method for Growth of Porous $BiVO_4$ Thin Films for Photoelectrochemical Water Oxidation . *J. Electrochem. Soc.* **2017**. *164*, H119. https://doi.org/10.1149/2.1321702jes.

(39) Wang, S.; Chen, P.; Yun, J. H.; Hu, Y.; Wang, L. An Electrochemically Treated $BiVO_4$ Photoanode for Efficient Photoelectrochemical Water Splitting. *Angew. Chemie - Int. Ed.* **2017**. *56*(29), 8500-8504. https://doi.org/10.1002/anie.201703491.

(40) Abdi, F. F.; Han, L.; Smets, A. H. M.; Zeman, M.; Dam, B.; Van De Krol, R. Efficient Solar Water Splitting by Enhanced Charge Separation in a Bismuth Vanadate-Silicon Tandem Photoelectrode. *Nat. Commun.* **2013**, *4*, 2195. https://doi.org/10.1038/ncomms3195.

(41) Kim, T. W.; Choi, K. S. Improving Stability and Photoelectrochemical Performance of BiVO4 Photoanodes in Basic Media by Adding a ZnFe2O4 Layer. *J. Phys. Chem. Lett.* **2016**, *7* (3), 447–451. https://doi.org/10.1021/acs.jpclett.5b02774.

(42) Palaniselvam, T.; Shi, L.; Mettela, G.; Anjum, D. H.; Li, R.; Katuri, K. P.; Saikaly, P. E.; Wang, P. Vastly Enhanced BiVO4 Photocatalytic OER Performance by NiCoO2 as Cocatalyst. *Adv. Mater. Interfaces* **2017**, *4* (19). https://doi.org/10.1002/admi.201700540.

(43) Kim, T. W.; Ping, Y.; Galli, G. A.; Choi, K. S. Simultaneous Enhancements in Photon Absorption and Charge Transport of Bismuth Vanadate Photoanodes for Solar Water Splitting. *Nat. Commun.* **2015**, *6*, 8769. https://doi.org/10.1038/ncomms9769.

(44) Zhong, M.; Hisatomi, T.; Kuang, Y.; Zhao, J.; Liu, M.; Iwase, A.; Jia, Q.; Nishiyama, H.; Minegishi, T.; Nakabayashi, M.; Shibata, N.; Niishiro, R.; Katayama, C.; Shibano, H.; Katayama, M.; Kudo, A.; Yamada, T.; Domen, K. Surface Modification of CoOx Loaded $BiVO_4$ Photoanodes with Ultrathin P-Type NiO Layers for Improved Solar Water Oxidation. *J. Am. Chem. Soc.* **2015**. *137*, 15, 5053–5060. https://doi.org/10.1021/jacs.5b00256.

(45) Pilli, S. K.; Furtak, T. E.; Brown, L. D.; Deutsch, T. G.; Turner, J. A.; Herring, A. M. Cobalt-Phosphate (Co-Pi) Catalyst Modified Mo-Doped BiVO4 Photoelectrodes for Solar Water Oxidation. *Energy Environ. Sci.* **2011**, *4* (12), 5028–5034. https://doi.org/10.1039/c1ee02444b.

(46) Liu, Y.; Wygant, B. R.; Kawashima, K.; Mabayoje, O.; Hong, T. E.; Lee, S. G.; Lin, J.; Kim, J. H.; Yubuta, K.; Li, W.; Li, J.; Mullins, C. B. Facet Effect on the Photoelectrochemical Performance of a $WO_3/BiVO_4$ Heterojunction Photoanode. *Appl. Catal. B Environ.* **2019**. *245*, 227-239. https://doi.org/10.1016/j.apcatb.2018.12.058.

(47) Chen, L.; Toma, F. M.; Cooper, J. K.; Lyon, A.; Lin, Y.; Sharp, I. D.; Ager, J. W. Mo-Doped $BiVO_4$ Photoanodes Synthesized by Reactive Sputtering. *ChemSusChem* **2015**, *8* (6), 1066–1071. https://doi.org/10.1002/cssc.201402984.

(48) Liu, J.; Chen, W.; Sun, Q.; Zhang, Y.; Li, X.; Wang, J.; Wang, C.; Yu, Y.; Wang, L.; Yu, X. Oxygen Vacancies Enhanced $WO_3/BiVO_4$ Photoanodes Modified by Cobalt Phosphate for Efficient Photoelectrochemical Water Splitting. *ACS Appl. Energy Mater.* **2021**, *4* (3).

ACS Author Version

https://doi.org/10.1021/acsaem.1c00145.

(49) Shi, Q.; Murcia-López, S.; Tang, P.; Flox, C.; Morante, J. R.; Bian, Z.; Wang, H.; Andreu, T. Role of Tungsten Doping on the Surface States in $BiVO_4$ Photoanodes for Water Oxidation: Tuning the Electron Trapping Process. *ACS Catal.* **2018**. 8, 4, 3331–3342. https://doi.org/10.1021/acscatal.7b04277.

(50) Gao, L.; Li, F.; Hu, H.; Long, X.; Xu, N.; Hu, Y.; Wei, S.; Wang, C.; Ma, J.; Jin, J. Dual Modification of a $BiVO_4$ Photoanode for Enhanced Photoelectrochemical Performance. *ChemSusChem* **2018**. *11*(15), 2502-2509. https://doi.org/10.1002/cssc.201800999.

(51) Chen, Z.; Jaramillo, T. F.; Deutsch, T. G.; Kleiman-Shwarsctein, A.; Forman, A. J.; Gaillard, N.; Garland, R.; Takanabe, K.; Heske, C.; Sunkara, M.; McFarland, E. W.; Domen, K.; Milled, E. L.; Dinh, H. N. Accelerating Materials Development for Photoelectrochemical Hydrogen Production: Standards for Methods, Definitions, and Reporting Protocols. *J. Mater. Research*. **2010.** *25* (1), 3-16. https://doi.org/10.1557/jmr.2010.0020.

(52) Trześniewski, B. J.; Smith, W. A. Photocharged $BiVO_4$ Photoanodes for Improved Solar Water Splitting. *J. Mater. Chem. A* **2016, 4**, 2919-2926. https://doi.org/10.1039/c5ta04716a.

(53) Baek, J. H.; Gill, T. M.; Abroshan, H.; Park, S.; Shi, X.; Nørskov, J.; Jung, H. S.; Siahrostami, S.; Zheng, X. Selective and Efficient Gd-Doped $BiVO_4$ Photoanode for Two-Electron Water Oxidation to H_2O_2. *ACS Energy Lett.* **2019**, *4* (3) 720-728. https://doi.org/10.1021/acsenergylett.9b00277.

(54) Peharz, G.; Dimroth, F.; Wittstadt, U. Solar Hydrogen Production by Water Splitting with a Conversion Efficiency of 18%. *Int. J. Hydrogen Energy* **2007**, *32*(15), 3248-3252. https://doi.org/10.1016/j.ijhydene.2007.04.036.

(55) Selamet, Ö. F.; Becerikli, F.; Mat, M. D.; Kaplan, Y. Development and Testing of a Highly Efficient Proton Exchange Membrane (PEM) Electrolyzer Stack. *Int. J. Hydrogen Energy* **2011**. *36* (17), 11480-11487. https://doi.org/10.1016/j.ijhydene.2011.01.129.

(56) Sapountzi, F. M.; Orlova, E. D.; Sousa, J. P. S.; Salonen, L. M.; Lebedev, O. I.; Zafeiropoulos, G.; Tsampas, M. N.; Niemantsverdriet, J. W. H.; Kolen'ko, Y. V. FeP Nanocatalyst with Preferential [010] Orientation Boosts Hydrogen Evolution Reaction in Polymer-Electrolyte Membrane Electrolyser. *Energy & Fuels* **2020**. *34,* 5, 6423–6429. https://doi.org/10.1021/acs.energyfuels.0c00793.

(57) Sapountzi, F. M.; Gracia, J. M.; Weststrate, C. J. (Kee. J.; Fredriksson, H. O. A.; Niemantsverdriet, J. W. Hans. Electrocatalysts for the Generation of Hydrogen, Oxygen and Synthesis Gas. *Progress in Energy and Combustion Science*. **2017.** *58*, 1-35. https://doi.org/10.1016/j.pecs.2016.09.001.

(58) Owens-Baird, B.; Xu, J.; Petrovykh, D. Y.; Bondarchuk, O.; Ziouani, Y.; González-Ballesteros, N.; Yox, P.; Sapountzi, F. M.; Niemantsverdriet, H.; Kolen'ko, Y. V.; Kovnir, K. NiP_2: A Story of Two Divergent Polymorphic Multifunctional Materials. *Chem. Mater.* **2019**, *31* (9). https://doi.org/10.1021/acs.chemmater.9b00565.

(59) Sekizawa, K.; Oh-Ishi, K.; Morikawa, T. Photoelectrochemical Water-Splitting over a

Accepted Version

Surface Modified p-Type Cr_2O_3 Photocathode. *Dalt. Trans.* **2020**, *49* (3). https://doi.org/10.1039/c9dt04296b.

(60) Jian, J.; Kumar, R.; Sun, J. Cu_2O/ZnO p-n Junction Decorated with NiOx as a Protective Layer and Cocatalyst for Enhanced Photoelectrochemical Water Splitting. *ACS Appl. Energy Mater.* **2020**, *3* (11), 8276–8284. https://doi.org/10.1021/acsaem.0c01198.

(61) Ta, C. X. M.; Furusho, Y.; Amano, F. Photoelectrochemical Stability of WO_3/Mo-Doped $BiVO_4$ Heterojunctions on Different Conductive Substrates in Acidic and Neutral Media. *Appl. Surf. Sci.* **2021**, *548*. https://doi.org/10.1016/j.apsusc.2021.149251.

Accepted Version